

1    **Spatial-temporal evolution of carbon emissions and their influencing**  
2    **factors in Shandong Province, China**

3

4    **Abstract**

5    The release of greenhouse gases has significantly impacted the global environment. With China's proposal of  
6    carbon peak and carbon neutrality, this study employs Shandong Province as a case study and conducts analysis from  
7    macro to micro levels, aiming to accurately identify the key issues to deal with. Firstly, this study adopts a bottom-up  
8    approach by integrating data related to land cover, CO<sub>2</sub>, CH<sub>4</sub>, and biofuels. Secondly, the estimation of county-scale  
9    carbon emissions is conducted using carbon emission factors. Then, spatial and temporal changes at provincial,  
10   municipal, county, and smaller scales are analyzed primarily through Gaussian distribution and spatial statistical  
11   methods. Finally, factor decomposition is performed from 2000 to 2020 using the generalized Divisia index method  
12   (GDIM). The results of the study reveal that: (1) The spatial distribution of county-scale exhibits primarily random  
13   patterns with occasional clusters or dispersion; (2) They are mainly concentrated in inland areas, showing a three-ring  
14   pattern, and at the municipal scale can also be divided into three echelons; (3) The main drivers come from GDP and  
15   energy consumption, and there is a slowdown in the growth rate, with a tendency represented by logarithmic function.  
16   Specifically, we discuss the spatial representation in geometry.

17   **Key words** carbon emission · spatial statistics · GDIM · county scale · spatial-temporal variation

18

19 **Introduction**

20 Dual carbon targets have become a hot term recently in China, which is the abbreviation for carbon peak and  
21 carbon neutrality. Nowadays, carbon emissions primarily originate from fossil fuels (Ajmi et al., 2015; Kasman &  
22 Duman, 2015), the central concern lies in their excessive magnitude, as is commonly known, it exacerbates the Earth's  
23 climate system warming and serves as a pivotal factor in intensifying the greenhouse effects (Baker et al., 2018; Gao  
24 et al., 2021) and represents a substantial global concern. Simultaneously, in China, the utilization of biofuels (straw,  
25 biomass pellets, etc.) has gradually gained momentum in certain rural regions. In this context, utilizing carbon  
26 emissions in Shandong Province as a case study, also holds implications for guiding other regions and this will enable  
27 us to enhance control measures and propose region-specific strategies for carbon reduction, thereby expediting the  
28 achievement of both carbon peak and carbon neutrality goals.

29 In response to this issue, researches on carbon emissions have attracted the interest of many scholars in recent  
30 years and have been conducted in a progressive manner (Chuai et al., 2015; Mishra et al., 2022; Rong et al., 2023).  
31 These encompass various aspects related to this topic. Firstly, in terms of the acquisition of data, Xing et al. (2022a)  
32 employed the Google Earth Engine (GEE) to acquire atmospheric data. In addition, the use of carbon emission factors,  
33 as per the reference indicators provided by Intergovernmental Panel on Climate Change (IPCC), provides a relatively  
34 simple and effective method for global calculations with reference value in regional studies. For example, Wang et al.  
35 (2017) conducted calculations on carbon emissions associated with energy consumption. Furthermore, the  
36 advancement of remote sensing has enhanced the efficiency and accuracy of data collection (Xing et al., 2022b).  
37 Secondly, in terms of analysis scale, the spatial and temporal dimensions primarily focus on larger scales. Shi et al.  
38 (2019) conducted a comprehensive study on carbon emissions in various provinces and municipalities across China.  
39 Zhang and Hong (2024) conducted a study in the Bohai Rim Region. Thirdly, in terms of analytical methods, GIS  
40 spatial analysis can employ methodologies to explore the spatiotemporal development patterns of carbon emissions  
41 effectively. Wang et al. (2022) employed the geographically and temporally weighted regression (GTWR) method  
42 conducted a spatiotemporal analysis to examine the variations in the influence of spatial structure on carbon emissions.  
43 Additionally, researches have extensively utilized indicators and models to explore the impact and driving factors of  
44 carbon emissions. In the study of Chen et al. (2020), a global carbon footprint pressure index was employed to elucidate  
45 the ecological repercussions of anthropogenic activities. Ma et al. (2019) employed logarithmic mean Divisia index  
46 decomposition method (LMDI) to establish a factor decomposition model for carbon emissions. Wang et al. (2019)  
47 adopted spatial Markov chain and observed the impact of Matthew and spatial spillover effect on the carbon emission  
48 intensity of Chinese urban. Other methods such as life cycle assessment' evaluation of the influence on carbon  
49 emissions (Yu et al., 2014).

50 However, attaining flawless research outcomes poses a formidable challenge. Carbon emission factors need to  
51 improve from a global to regional perspective to enhance its adaptability at the local level. Additionally, conducting  
52 calculations of carbon emissions at smaller spatial scales, such as counties, remains challenging due to insufficient  
53 support from relevant basic data and acquisition methods. Consequently, Zhang et al. (2023) have explored the  
54 relationship between carbon emissions and nighttime light data, by employing long-term DMSP/OLS and NPP/VIIRS  
55 nighttime light data fitting techniques, they successfully estimated carbon emissions at the county level. This approach  
56 enables an assessment of carbon emissions starting from higher administrative levels down to individual counties (top-  
57 down). Furthermore, when considering the relationship between humans and the environment, it is imperative to  
58 account for both regional similarities and global heterogeneity, the connection and independence of phenomena are  
59 pivotal attributes, exemplified by the investigation of Zhu et al. (2022) into the correlation between land cover change  
60 and carbon emissions, temporal continuity and non-stationarity should also be taken into consideration to ensure a  
61 thorough and comprehensive analysis.

62 In light of the aforementioned contents, this study primarily employs grid data to compute carbon emissions from  
63 subnational administrative units and aggregate them to higher-level administrative regions (bottom-up), based on this,  
64 the calculation results will be examined for data quality and errors through Gaussian distribution. Subsequently,  
65 modeling through spatial relationships, spatial statistical analysis will be conducted at various administrative levels,  
66 ranging from provincial and municipal to county and sub-county scales. Finally, Generalized Divisia index method  
67 (GDIM) will be employed to unveil various phenomena and factors influencing carbon emissions. In addition, some  
68 basic statistical analysis methods such as data fitting functions will also be employed to forecast future carbon  
69 emissions and the velocity as well as acceleration of its spatiotemporal changes.

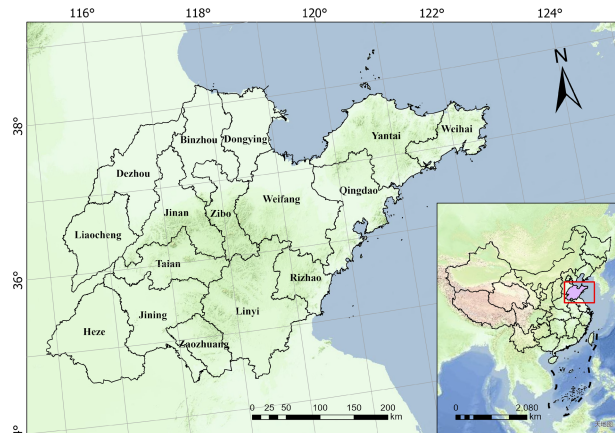
70 This study has the following contributions. Firstly, this study employs a method of proof by contradiction or

71 indirect, which can be simply explained as analyzing the combined impact of A and B, then analyzing the individual  
72 impact of A, and then comparing the differences obtained to determine the impact caused by B. The utilization of this  
73 approach is applicable in situations where direct analysis of B poses challenges. This will be used in hotspot analysis.  
74 Secondly, there will be a further discussion on the spatial representation in geometry and a more rigorous demonstration  
75 of confidence or significance level in spatial statistics. Thirdly, we conducted an examination of the changes in both  
76 Global Moran's I and Z-score. This allows for an understanding of local distribution patterns at a global level, thereby  
77 corresponding to localized analyses in Anselin Local Moran's I.

## 78 Materials and methods

### 79 Study area

80 Shandong Province, including 16 prefecture-level cities and 136 county-level administrative divisions, its  
81 geographical coordinates range from  $34^{\circ}23'$  to  $38^{\circ}17'$  north latitude and from  $114^{\circ}48'$  to  $122^{\circ}42'$  east longitude (Fig.1),  
82 situating it in the coastal region downstream of the Yellow River Basin (YRB) in China (Fan et al., 2020). This province  
83 is geographically divided into two distinct parts: the Shandong Peninsula and its inland region. Shandong Province  
84 exhibits diverse landforms characterized by plains covering around 55% of its territory while hills (13.2%) and  
85 mountains (15.5%) are mainly concentrated in central regions.



86  
87 **Fig.1** Study area geographic location

### 88 Data sources

89 This study employs land cover, CO<sub>2</sub>, CH<sub>4</sub> and biofuels data to calculate carbon emissions.

90 The land cover data (2000, 2005, 2010, 2015, 2020) in this study is derived from the China Land Cover Dataset  
91 (CLCD), it comprises nine land cover categories, cropland, forest, shrub, grassland, water, snow/ice, barren,  
92 impervious, and wetland. Based on 5,463 visual samples, the CLCD achieves an overall accuracy of 79.31% (Yang &  
93 Huang, 2021). However, considering the smaller research scope within Shandong Province compared to the entire  
94 country and to better align with this study's focus on regional conditions specifically in Shandong Province, a  
95 reclassification of these nine land cover categories was performed. Forest and shrub were merged into a single category  
96 called forest; water along with snow and ice as well as wetland were grouped together as water; barren land and  
97 impervious were classified as unnatural land; while cropland and grassland remained separate resulting in a total of  
98 five distinct types of land cover. This data is primarily used for land cover change analysis and the calculation of direct  
99 carbon emissions (DCE).

100 Partial data on carbon emissions: EDGAR (Emissions Database for Global Atmospheric Research), a  
101 collaboration between the European Commission, Joint Research Centre, the International Energy Agency  
102 ([https://edgar.jrc.ec.europa.eu/dataset\\_ghe80](https://edgar.jrc.ec.europa.eu/dataset_ghe80) (accessed on 9 May 2024)), provides carbon emissions from the use of  
103 fossil fuels and materials, as well as from biofuels (Excluding large-scale biomass burning, grassland burning, forest  
104 fires, and land types change). The data is provided in NETCDF format, with a spatial resolution of  $0.1^{\circ} \times 0.1^{\circ}$  grid per  
105 year. This part of the data is primarily used for estimating indirect carbon emissions (ICE).

106 Carbon emissions

107 According to the emission factor method proposed by IPCC, in this study, we categorized the total carbon  
108 emissions (TCE) into direct and indirect parts, DCE and ICE.

109 DCE pertain to the release of carbon resulting from various land types. The annual DCE for a kind of land type  
110 can be determined by multiplying the corresponding carbon emission factor with the area of that land.

$$C_m = A_m * \delta_m \quad (1)$$

111 Where  $m$  is the land type,  $C_m$  is the DCE associated with a specific land type,  $A_m$  is the area of land, and  $\delta_m$  is the  
112 carbon emission factor pertaining to a certain type of land.

113 Considering that Shandong Province is situated in the eastern part of YRB, while also being in close proximity to  
114 the Beijing-Tianjin-Hebei region, we have assigned weights based on previous research findings (Chen et al., 2024;  
115 Guo et al., 2023), 0.35 and 0.65 respectively. The results are presented in Table 1.

117 **Table 1** Carbon emission factors of different land types

Type	Factor (Unit: t/(hm <sup>2</sup> ·a))
Cropland	0.4726
Forest	-0.6015
Grassland	-0.0213
Water	-0.2445
Unnatural land	-0.0050

118 ICE refer to the release of carbon caused by human activities. in this study, ICE are based on the EDGAR database.

119 TCE are net emissions, encompassing DCE from various land types as well as ICE from various energy sources.  
120 In this study, 1 t = 1000 kg.

$$C = \sum C_n + \sum C_m \quad (2)$$

121 Where  $C$  is the TCE,  $\sum C_n$  is the total ICE, and  $\sum C_m$  is the total DCE.

124 Data Quality and Error Verification

125 The majority of phenomena in the world conform to Gaussian distribution, as observed in measurement errors,  
126 regional temperatures and precipitations, etc. These variables approximately adhere to Gaussian distribution both  
127 before or after undergoing data transformation, such as logarithmic, exponential, and square transformations. So, it can  
128 be inferred that the TCE may also follow a Gaussian distribution.

129 The deviation of data from a Gaussian distribution can be assessed and potential outliers or anomalies identified  
130 by employing various statistical indicators, such as mean, median, kurtosis and skewness.

$$K = \frac{\frac{1}{n} \sum_{i=1}^n (x_i - \bar{x})^4}{\left( \frac{1}{n} \sum_{i=1}^n (x_i - \bar{x})^2 \right)^2} \quad (3)$$

$$S = \frac{\frac{1}{n} \sum_{i=1}^n (x_i - \bar{x})^3}{\left( \frac{1}{n} \sum_{i=1}^n (x_i - \bar{x})^2 \right)^2} \quad (4)$$

131 In equations (3) and (4),  $K$  is kurtosis,  $S$  is skewness,  $n$  is the sample size, and  $x_i$  is the value of the i-th sample,  
132 with  $\bar{x}$  being the mean of the samples.

135 Spatial Correlation

136 *Spatial relationship modeling*

137 The spatial relationship in this study is represented by the square of the inverse Euclidean distance, and the  
138 influence between elements diminishes as the distance increases. On this basis, the spatial weight matrix (SWM) is  
139 constructed as a spatial relationship model (Getis & Aldstadt, 2004; Mitchell, 2005).

140 Considering the limited connectivity with neighboring provinces at provincial boundaries, counties located on the

border may experience certain impacts. The distance threshold is approximately 44000 meters (close to the average distance determined by subsequent Incremental Spatial Autocorrelation).

It should be stated that broad spatial relationships may do not proper reflect the true spatial relationship. For instance, if TCE are concentrated within one county or district, they may only influence each other within this specific area and have no bearing on other counties or districts. When describing spatial relationships on a larger scale, the ability to depict local variations diminishes, potentially introducing bias in these relationships. By normalizing weights based on the ratio of individual weight to total weight, the advantages are gained: The weights range from 0 to 1, summing up to a total of 1. This enables the adjustment of weights between two factors while preserving their spatial relationship, thereby minimizing discrepancies arising from varying numbers of neighboring factors, both at the boundary and within the interior.

### 151 Global Moran's I

152 The Global Moran's I is employed to assess the spatial autocorrelation at a macroscopic level (Anselin, 2010).  
153 The clusters, dispersion, or randomness of the results could be determined through confidence tests conducted on the  
154 P-value and Z-score.

$$155 I = \frac{n \sum_{i=1}^n \sum_{j=1}^n w_{i,j} z_i z_j}{S_0 \sum_{i=1}^n z_i^2} \quad (5)$$

$$156 S_0 = \sum_{i=1}^n \sum_{j=1}^n w_{i,j} \quad (6)$$

$$157 z_i = x_i - \bar{x} \quad (7)$$

158 Where  $n$  is the total number of elements,  $w_{i,j}$  is the spatial weight between  $i$  and  $j$ ,  $x_i$  is the attribute value of an  
159 element,  $\bar{x}$  is the mean value of all elements,  $S_0$  is the sum of all spatial weights, and  $I$  is the Moran's index.

### 160 Anselin Local Moran's I - LISA

161 In LISA (Anselin, 1995), spatial clusters are where the high values are surrounded by other high values (HH) and  
162 low values are surrounded by other low values (LL); Outliers are where the high values are surrounded by low values  
163 (HL) and vice versa (LH). However, it is essential for the P value to be sufficiently small in order to reject the null  
164 hypothesis and satisfy the testing conditions.

$$165 I = \frac{x_i - \bar{x}}{S_i^2} \sum_{j=1, j \neq i}^n w_{i,j} (x_j - \bar{x}) \quad (8)$$

$$166 S_i^2 = \frac{\sum_{j=1, j \neq i}^n (x_j - \bar{x})^2}{n-1} \quad (9)$$

167 Where  $n$  is the total number of elements,  $w_{i,j}$  is the spatial weight between  $i$  and  $j$ ,  $x_i$  is the attribute value of an  
168 element,  $\bar{x}$  is the mean value of elements,  $I$  is the local Moran's index.

169 In this study, the significance test is conducted at a confidence level of 95%, and P-value below 0.05 is considered  
170 statistically significant. Subsequently, spatial patterns are further determined using local Moran's index and Z-score.  
171 To ensure the accuracy in reflecting the true spatial distribution pattern, a total of 10,000 calculations are conducted,  
172 with one calculation being essential and the remaining 9,999 calculations serving for verification purposes.

### 173 Hotspot Analysis

174 The term "hot spot" refers to HH, while "cold spot" refers to LL, also it is imperative to subject this classification  
175 to a significance test. Consequently, this methodology exhibits certain resemblances with LISA. However, there is still  
176 a certain purpose in using this method.

177 By converting grid data ( $0.1^\circ \times 0.1^\circ$ ) of ICE into points and employing optimized hotspot analysis at a sub-county  
178 scale, the influence of factors such as DCE and analysis scale can be assessed by comparing the outcomes with LISA's  
179 evaluation of TCE. This can be accomplished through a reverse or indirect proof.

#### 180 (1) Incremental Spatial Autocorrelation - ISA

181 Through progressively extends the distance for Global Moran's I, while quantifying the level of spatial clusters at  
182 each distance increment, then the ISA will generate a line graph where the peak indicates the optimal distance that  
183 facilitates significant spatial clusters (Ran et al., 2021), serving as the range for hotspot analysis.

184 (2) Getis-Ord Gi\*

185 The Gi\* (Getis & Ord, 1992) is a Z-score variant, where larger positive values indicate stronger clusters of HH  
186 and larger negative values indicate stronger clusters of LL.

$$187 G_i^* = \frac{\sum_{j=1}^n w_{i,j} x_j - \bar{x} \sum_{j=1}^n w_{i,j}}{S \sqrt{\frac{n \sum_{j=1}^n w_{i,j}^2 - (\sum_{j=1}^n w_{i,j})^2}{n-1}}} \quad (10)$$

$$188 \bar{x} = \frac{\sum_{j=1}^n x_j}{n} \quad (11)$$

$$189 S = \sqrt{\frac{\sum_{j=1}^n x_j^2}{n} - (\bar{x})^2} \quad (12)$$

190 Where  $n$  is the number of elements,  $x_j$  is the attribute value of  $j$ ,  $w_{i,j}$  is the spatial weight between  $i$  and  $j$ .

191 Generalized Divisia Index Method - GDIM

192 *Calculating indicators and Kaya identity*

193 The study selects four indicators: TCE ( $10^4$  tons), Energy Consumption (EC, converted to  $10^4$  tons of standard  
194 coal), GDP ( $10^8$  ¥), Population ( $10^4$ ), refer to the Statistical Yearbook of Shandong Province.

195 **Table 2** Statistical Indicators of Shandong Province

Year	EC	TCE	GDP	Population
2000	12513.21	44045.96	8278.06	8997.00
2005	25687.50	74493.72	15947.51	9248.00
2010	36357.25	94662.02	33922.49	9579.00
2015	39331.60	109180.93	55288.79	9866.00
2020	43649.00	119516.65	73129.00	10165.00

196  
197 The TCE commences by formulating the Kaya identity (Kaya, 1990), a multiplicative equation that dissects TCE  
198 into a product of various indicators.

199 Assuming there is  $Z = f(X) = f(X_1, X_2, \dots, X_n) = X_1 * X_2 * \dots * X_n$ ,  $X_i = X_i(t)$  changes over time. Through  
200 the application of calculus operations, we can derive the change  $\Delta Z$  and its constituent elements across various time  
201 intervals spanning from  $t_0$  to  $t_1$ .

$$202 \Delta Z = \Delta Z[X_1] + \Delta Z[X_2] + \Delta Z[X_3] + \dots + \Delta Z[X_n] \quad (13)$$

203 The vector representation can be employed for each individual component.

$$204 \begin{aligned} \Delta Z &= \langle \Delta Z[X_1], \dots, \Delta Z[X_n] \rangle \\ &= \langle \int_{t_0}^{t_1} f'_1 X'_1 dt, \dots, \int_{t_0}^{t_1} f'_n X'_n dt \rangle \\ &= \int_{t_0}^{t_1} \langle f'_1, \dots, f'_n \rangle d\mathbf{X} \\ &= \int_{t_0}^{t_1} \nabla \mathbf{Z}^T d\mathbf{X} \end{aligned} \quad (14)$$

205 Reveal the proof in Generalized Divisia Index Method (Vaninsky, 2014).

206 In this paper, it is actually constructed as:

$$207 \begin{aligned} C &= \frac{C}{E} * \frac{G}{P} * \frac{E}{G} * P \\ &= G * \frac{C}{G} \\ &= E * \frac{C}{E} \\ &= P * \frac{C}{P} \end{aligned} \quad (15)$$

$$208 \begin{aligned} Z &= X_4 * X_5 * X_7 * X_8 \\ &= X_1 * X_2 \\ &= X_3 * X_4 \\ &= X_5 * X_6 \end{aligned} \quad (16)$$

209 Among the various forms of its changes, each factor carries different meanings as Table 3. By standardizing using  
 210 ratios, it is possible to eliminate unit differences and mitigate the impact of varying indicator sizes on the outcomes.

211 **Table 3** Comparison of Indicator Meanings

Variable	Meaning
Z=C=C1/C0	TCE at the end period relative to the base period, TCE growth rate
X1=G=G1/G0	GDP growth rate
X3=E=E1/E0	EC growth rate
X5=P=P1/P0	Population growth rate
X2=C/G	Economic carbon intensity
X4=C/E	Energy carbon intensity
X6=C/P	Per capita carbon emission intensity
X7=G/P	Per capita GDP
X8=E/G	Unit energy dependency rate

212  
 213 However, this equation has certain limitations, such as the potential for EC to not accurately reflect variations in  
 214 TCE. It could be attributed to advancements in production processes, but it is crucial to avoid overly idealistic  
 215 assumptions.

216  $C = \frac{C}{E} * E$  (17)

217  $C = \frac{C}{2E} * 2E$  (18)

218 The range of results could be refined through the addition of constraints, thereby enhancing precision. For  
 219 instance, these is an equation system:

220  $C = \frac{C}{E} * E$  (19)

221  $E - 1 = 0$  (20)

222 In this way, the  $2E - 1 \neq 0$  is ruled out.

223 *Construction of GDIM*

224 To facilitate expression, construct  $Z = f(X)$ ,  $\Phi(X) = 0$  based on equation (15), (16).

$$\begin{aligned} Z &= X_1 * X_2 \\ X_1 * X_2 - X_3 * X_4 &= 0 \\ X_1 * X_2 - X_5 * X_6 &= 0 \\ X_1 - X_5 * X_7 &= 0 \\ X_3 - X_1 * X_8 &= 0 \end{aligned} \quad (21)$$

225 Construct gradient vector and Jacobian matrix through partial derivative calculations.

226  $\nabla Z = (X_2, X_1, 0, 0, 0, 0, 0, 0)^T$  (22)

$$\Phi_X = \begin{pmatrix} X_2 & X_1 & -X_4 & -X_3 & 0 & 0 & 0 & 0 \\ X_2 & X_1 & 0 & 0 & -X_6 & -X_5 & 0 & 0 \\ 1 & 0 & 0 & 0 & -X_7 & 0 & -X_5 & 0 \\ -X_8 & 0 & 1 & 0 & 0 & 0 & 0 & -X_1 \end{pmatrix}^T \quad (23)$$

227 The geometric interpretation of the equation system  $\Phi(X) = 0$  in Equation (21) represents surfaces passing  
 228 through the origin in space, which is independent but not necessarily orthogonal. By employing Vaninsky's formula,  
 229 vectors are projected onto the defined surfaces to form components  $\Delta Z[\Phi(X)]$ .

230  $\Delta Z[\Phi(X)] = \int_L \nabla Z^T (I - \Phi_X \Phi_X^+) dX$  (24)

231  $\Phi_X^+ = (\Phi_X^T \Phi_X)^{-1} \Phi_X^T$  (25)

238  $\mathbf{d}\mathbf{X} = \text{diag}(X'_1, \dots X'_n)$  (26)

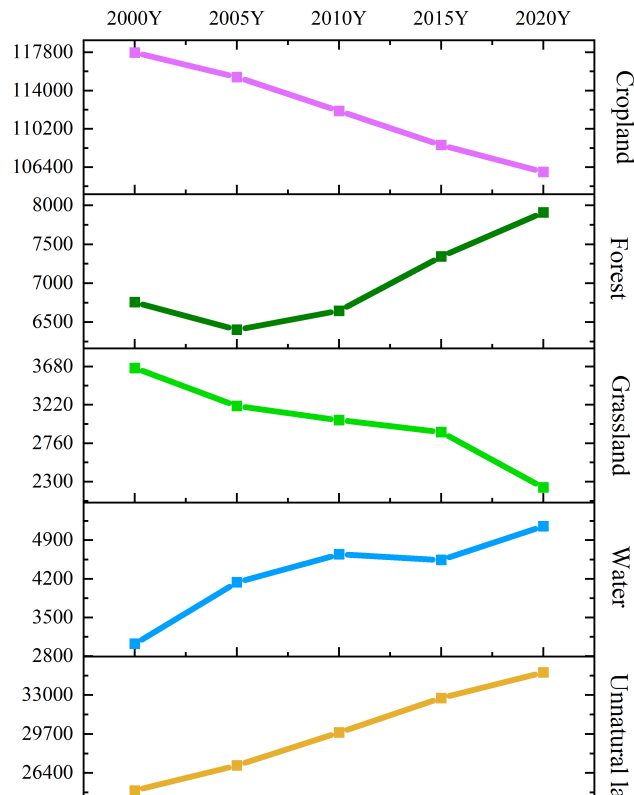
239 Where  $L$  is the time span from the base period to the end period, the  $I$  is an identity matrix, and  $X_i$  is assumed to  
240 be an exponential function that varies with time.

241 The process can be described as projecting the vector obtained from the initial multiple indicators onto a new set  
242 of coordinate axes, resulting in the formation of a novel vector.

## 243 Results and Discussion

### 244 Land cover change

245 The Fig. 2 presents the land cover changes in Shandong Province from 2000 to 2020 ( $\text{km}^2$ ). As a prominent  
246 agricultural province, Shandong holds a pivotal position in terms of crop. However, over the past two decades, the  
247 accelerated process of urbanization has led to a declining trend in the extent of crop, posing challenges to food security  
248 strategies. Conversely, there has been an increase in unnatural land. The forests and water have exhibited an overall  
249 upward trend and the grassland is gradually declining, however, it is important to note that these three categories cannot  
250 be compared on the same level as cropland.



251 **Fig. 2 Land cover changes**

252

### 253 Spatiotemporal change of carbon emissions

### 254 Overall level

255 Fig. 3 shows that DCE is primarily influenced by crop, and its change trend aligns with that. When considering  
256 land cover change, factors such as a decrease in the crop area and improvements in cultivation conditions contribute  
257 to the reduction in DCE. Forests serve as the primary carbon sink, however, due to their smaller coverage, their impact  
258 on reduction is relatively limited. The quantities and trends of carbon sinks in water and unnatural lands exhibit  
259 similarities, while grasslands demonstrate an opposite pattern. Furthermore, the changes in DCE for each land type are  
260 consistent with their respective alterations in area.

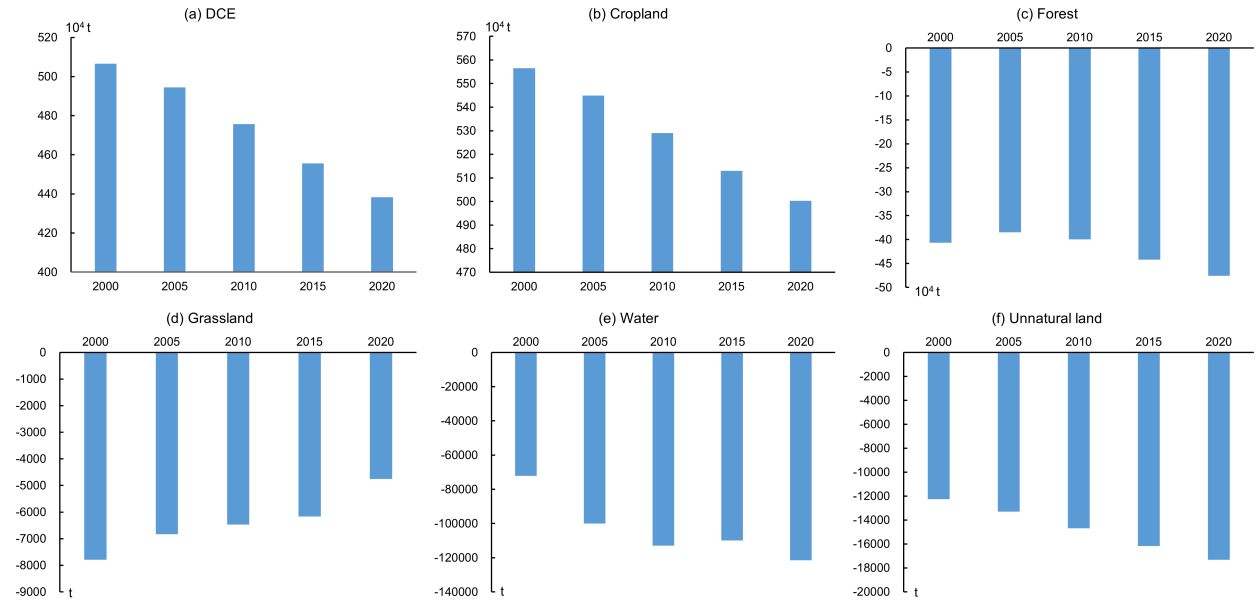


**Fig. 3** DCE from different types of land

261  
262

263 By integrating the findings from Fig. 4 and Fig. 5, it becomes evident that both the quantity and variability of  
264 TCE closely resemble those of ICE. Furthermore, a gradual decline in DCE in Fig. 3 is accompanied by a progressive  
265 increase in ICE, the magnitude of ICE has significantly surpassed that of DCE, leading to an escalating proportion of  
266 ICE.

267 The TCE from 2000 to 2020 were modeled using a logarithmic function, the  $R^2=0.9991$ , providing an overall  
268 approximation due to the 5-year time resolution employed in this study. However, conducting more detailed research  
269 may unveil localized fluctuations and anomalies.

$$y = 47184 * \ln(x) + 43201 \quad (27)$$

$$\frac{dy}{dx} = \frac{47184}{x} \quad (28)$$

270 Where  $x$  is different years, such as 2000 ( $x=1$ ), 2005 ( $x=2$ ), and 2010 ( $x=3$ ).  
271

272 Fig. 5 demonstrates the application of this function for extrapolating TCE in 2025, with black error lines  
273 representing a deviation range of  $\pm 10\%$ . Simultaneously, it can be observed via derivative calculations that the rate of  
274 growth in TCE is decelerating.  
275

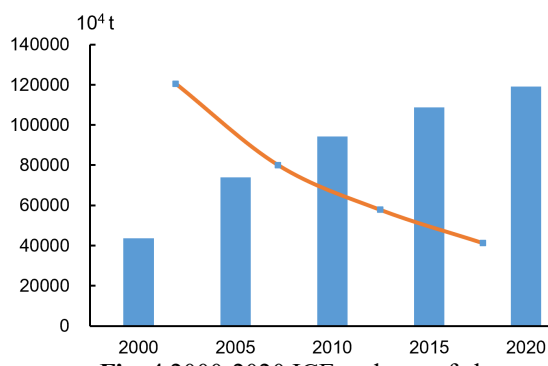


**Fig. 4** 2000-2020 ICE and rate of change

276  
277

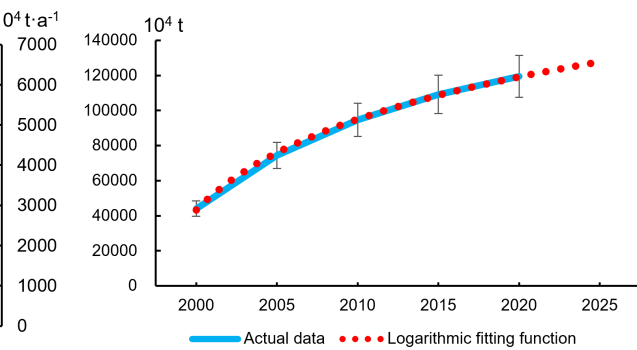


**Fig. 5** 2000-2020 TCE and fitting function

278 Furthermore, Vaninsky employs a time-varying exponential model in GDIM. Given the inverse relationship  
279 between logarithmic and exponential functions (as strictly monotonic functions possess inverse functions), their  
280 conversion becomes feasible. This implies that subsequent GDIM calculations can utilize exponential functions.

281 *Local level*

282 Fig. 6 illustrates the TCE at the municipal level. It is evident that nearly every prefecture-level city has witnessed

283 an upward trend. Binzhou and Weifang, both belonging to the first tier, exhibit the most substantial increase and highest  
 284 levels of TCE. Notably, Jinan, Jining, Liaocheng, Linyi, Rizhao, Taian, Zibo form the second tier. In contrast, Dezhou,  
 285 Dongying, Heze, Qingdao, Weihai, Yantai, Zaozhuang demonstrate relatively stable TCE and constitute the third tier.

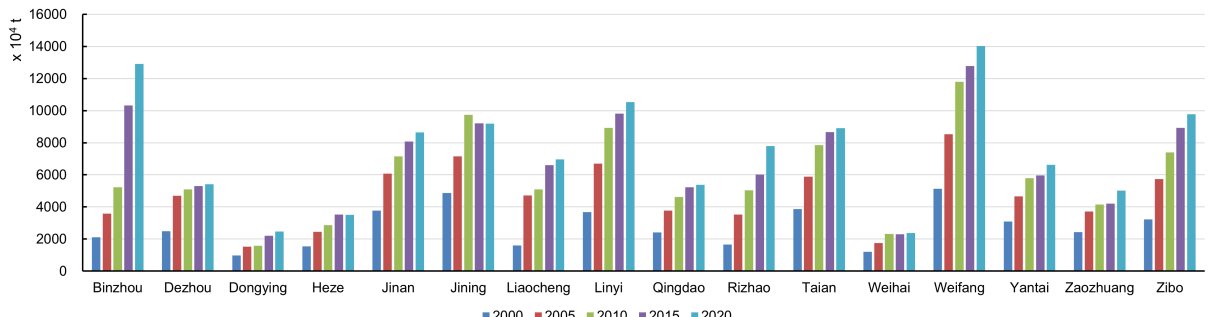


Fig. 6 2000-2020 municipal TCE dynamics

288 Fig. 7 illustrates the TCE at the county level. Following Jenks' natural breaks classification method, approximate  
 289 integer values are assigned to represent the natural breakpoints for dividing TCE in county-level of Shandong from  
 290 2000 to 2020 into 10 levels.

291 The TCE in Shandong is increasing in a growing number of counties. Overall, there is a pattern with more central  
 292 areas and fewer surrounding areas, where the western inland regions surpass the eastern peninsula, and the southeast  
 293 exhibits higher emissions compared to the northwest. In 2020, the central region comprises Zouping in Binzhou;  
 294 Licheng, Zhangqiu, Laiwu in Jinan; Linqu, Qingzhou in Weifang; but excludes Boshan in Zibo. The second ring:  
 295 Dongying district in Dongying; Bincheng district in Binzhou; Renping and Dongchangfu in Liaocheng; Feicheng and  
 296 Ningyang in Taian; Zoucheng in Jining; Pingyi and Lanshan in Linyi; Juxian in Rizhao; Anqiu, Weicheng, Shouguang  
 297 in Weifang. The third ring encompasses scattered locations such as Wudi on the boundary of Binzhou; Decheng in  
 298 Dezhou; Mudan in Heze; Tengzhou, Shanting, Shizhong, Taierzhuang in Zaozhuang; Lanshan in Rizhao; Chengyang  
 299 in Qingdao; Huancui in Weihai; Qixia, Longkou in Yantai.

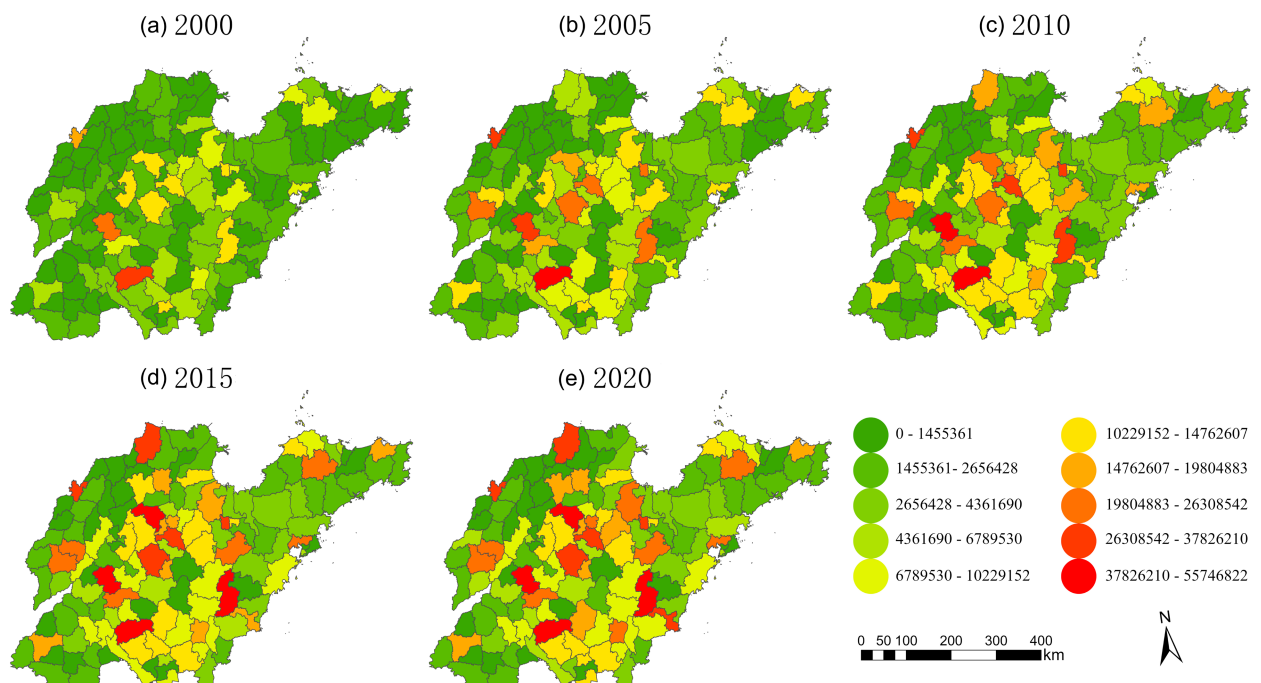


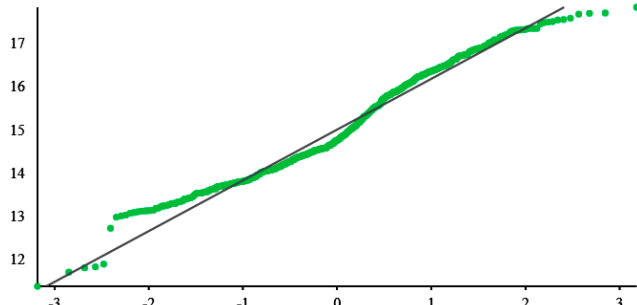
Fig. 7 2000-2020 county-level dynamics of TCE

300 301 The ocean, referred to as "blue carbon," plays a pivotal role in the absorption of carbon (Tang et al., 2018). In  
 302 close proximity to the ocean, the eastern regions exhibit lower levels of TCE, which may be attributed to the influence  
 303

304 of oceanic carbon sinks. Additionally, Dezhou, Liaocheng, and Heze situated within the western boundary arc  
305 distribution are top three grain producers. In comparison to developed industrial and commercial areas in central, these  
306 agricultural regions demonstrate significantly reduced levels of TCE.

307 Normality of TCE

308 To examine the logarithmic transformation of TCE from 2000 to 2020, a QQ plot was employed for comparison  
309 with the standard normal distribution, as depicted in Fig. 8.



310  
311 **Fig. 8** Comparison between TCE after logarithmic transformation and normal distribution

312 After calculation, the mean is 15.0, the median is 14.7, with a skewness of 0.23 and kurtosis of 2.4. After the  
313 logarithmic transformation, the TCE exhibits a closer resemblance to a Gaussian distribution. Given that Gaussian  
314 distribution can effectively capture randomness, this suggests that the data is generated through the combined influence  
315 of multiple random factors, thereby minimizing artificially induced generation, the data quality can be deemed  
316 acceptable.

317 The data conforms well to a Gaussian distribution except at the upper part of the tail. The data at these may be  
318 influenced by outliers or unexpected values, where TCE values are generally smaller and exist a certain degree of  
319 deviation. It may be due to the fluctuations caused by limitations of early data collection techniques, because the early  
320 TCE are usually smaller, such as 2005 in Fig. 7.

321 Spatiotemporal pattern of TCE

322 *Global pattern*

323 In the results of Global Moran's I, Table 4, the p-values exhibit relatively high values for each year, indicating a  
324 lack of statistical significance and the null hypothesis of random distribution cannot be rejected. Simultaneously,  
325 Moran's I tends towards 0, suggesting a closer resemblance to randomness. The absolute values of Z scores are small,  
326 implying weak levels of clusters or dispersion. Consequently, overall, the spatial distribution demonstrates a pattern  
327 consistent with random distribution at a global level.

328 **Table 4** Global Moran's I calculation results

Time	Moran's I	Z-Score	P-value
2000	-0.03081	-0.40097	0.68844
2005	-0.01996	-0.21026	0.83346
2010	0.01646	0.39783	0.69075
2015	0.01157	0.31392	0.75358
2020	0.00823	0.25897	0.79566

329  
330 In Fig. 9, the Moran's I and Z scores exhibited an increasing trend from 2000 to 2010, transitioning from negative  
331 to positive values thereafter. While displaying an overall random distribution, but there is a trend of shifting slightly  
332 from dispersion to clusters. The subsequent decline in positive values after 2010 tended to lean more towards  
333 randomness.

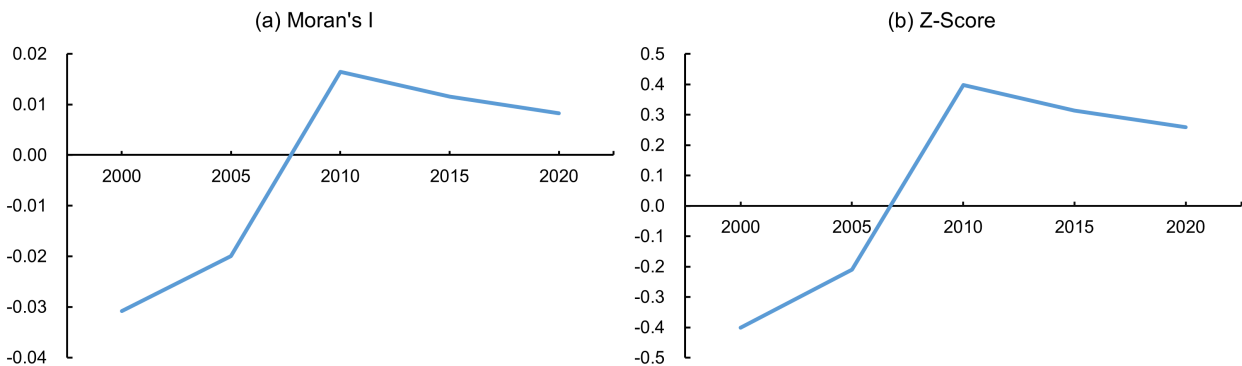


**Fig. 9** Changes in Moran's I and Z-score

### 336 Region pattern

337 At the county scale, Fig. 10, there are limited and relatively dispersed instances of clusters and outliers. These  
 338 occurrences primarily manifest in the inland regions of Shandong, while they are less prevalent in the peninsula area.  
 339 Following 2010, there has been a decline in clusters but an increase in outliers, aligning with the changes of Global  
 340 Moran's I and Z-Score in Fig. 9.

341 Before 2010, HH was primarily concentrated in Zaozhuang Tengzhou and Jining Qufu, regions characterized by  
 342 high TCE, resulting in clusters of elevated values. After 2010, Zhangqiu in Jinan, Zhoucun in Zibo, and Junan in Linyi  
 343 also experienced an increase in HH. LL predominantly occurred in Shanxian of Heze to the southwest, Rushan of  
 344 Weihai to the northeast, as well as border areas of Dezhou and Binzhou to the northwest and Jinan. HL was mainly  
 345 observed in Wudi of Binzhou to the northwest, Decheng, Qihe of Dezhou, as well as Licheng of Jinan. LH was  
 346 primarily situated near central regions such as Gaoqing of Zibo and Boshan, Changle of Weifang, and in 2020,  
 347 Donggang emerged within Rizhao, but some LH disappeared due to increased TCE from certain counties previously  
 348 located within Jining. However, for most regions, clusters and outliers are not significant.

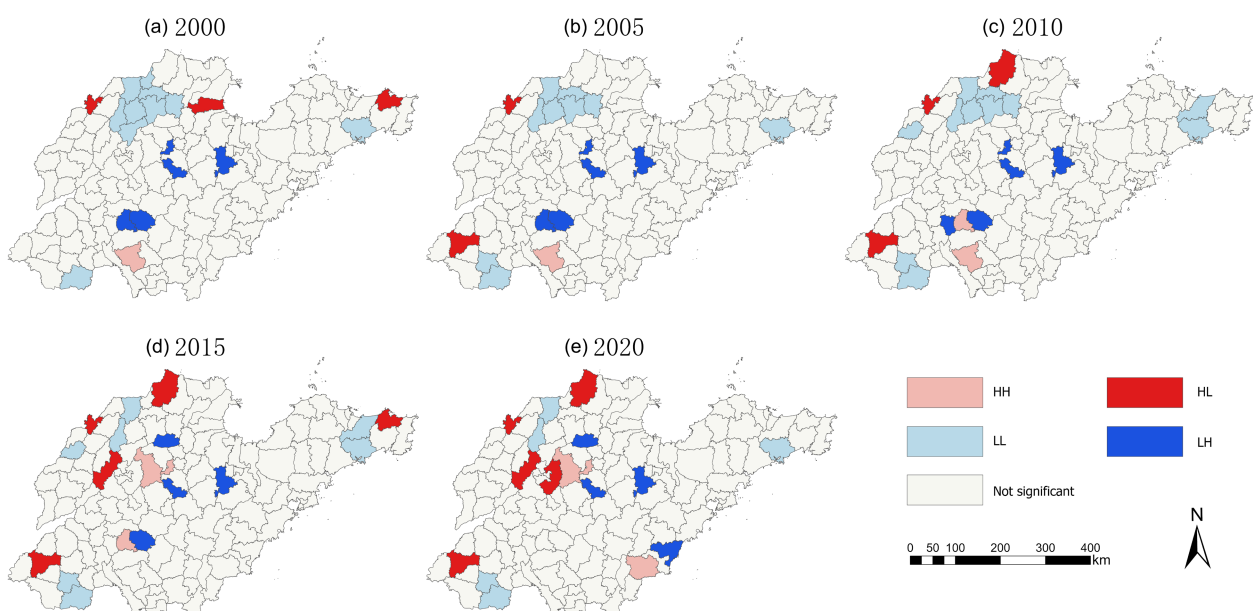
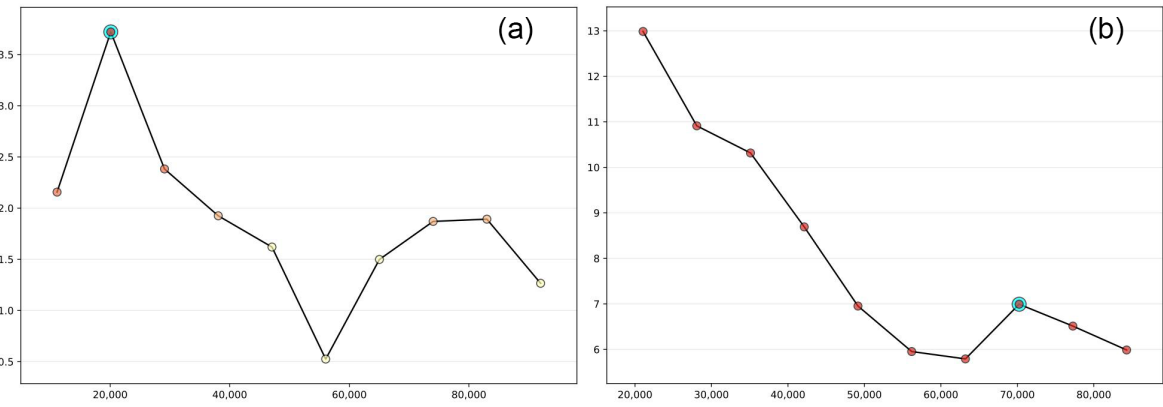


**Fig. 10** 2000-2020 clusters and outliers' distribution

### 351 Impacts of DCE, ICE and scale on distribution patterns

352 In the Fig. 11, the left graph (a) illustrates the ISA in 2000. The horizontal axis represents distance (m), while the  
 353 vertical axis represents Z-scores. The maximum value indicates the most significant distance that facilitates spatial  
 354 clusters, which serves as the range for hot spot analysis. However, there are instances that identifying a distinct distance  
 355 promoting spatial clusters becomes challenging, and extreme values may not necessarily be optimal, as observed in

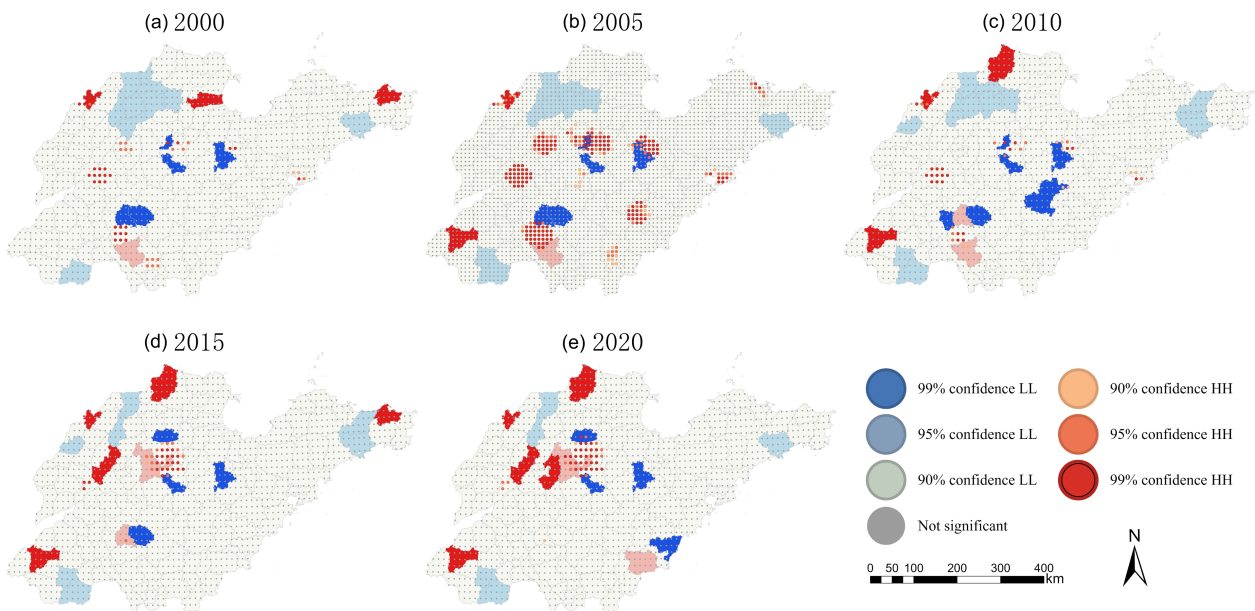
356 2005, but it was only this year that was not optimal, this may also be attributed to the deviation observed towards the  
 357 upper part of the tail in Fig. 8, leading to anomalous circumstances. In such cases, we employ the average distance to  
 358 the 30 nearest neighbors as the analytical range.



359  
 360 **Fig. 11** Incremental spatial autocorrelation between 2000 and 2005

361 According to hotspot analysis, the findings exhibit certain similarities with LISA, thereby offering potential for  
 362 mutual complementation and correction. Fig. 12 shows that, except for 2005, LISA and hot spot analysis generally  
 363 demonstrate close spatial patterns. However, in 2005, there was also a lack of ISA, posing challenges in identifying an  
 364 appropriate domain range for analysis.

365 By conducting  $Gi^*$  to examine the spatial distribution patterns of ICE, it is possible to infer DCE and evaluate the  
 366 impacts associated with different analytical scales by comparing them with LISA on TCE. This suggests that the DCE  
 367 and the impact of analysis scales are predominantly observed in Jinan Pingyin, Taian Feicheng. In other regions, the  
 368 outcomes of LISA and hot spot analysis primarily encompass neighboring or surrounding counties, which may  
 369 represent areas where county-level assessment closely reflects the actual influence of carbon emissions, also, the ICE  
 370 can to a large extent obscure the impact of DCE.



371  
 372 **Fig. 12** 2000-2020 changes in  $Gi^*$  in Shandong Province

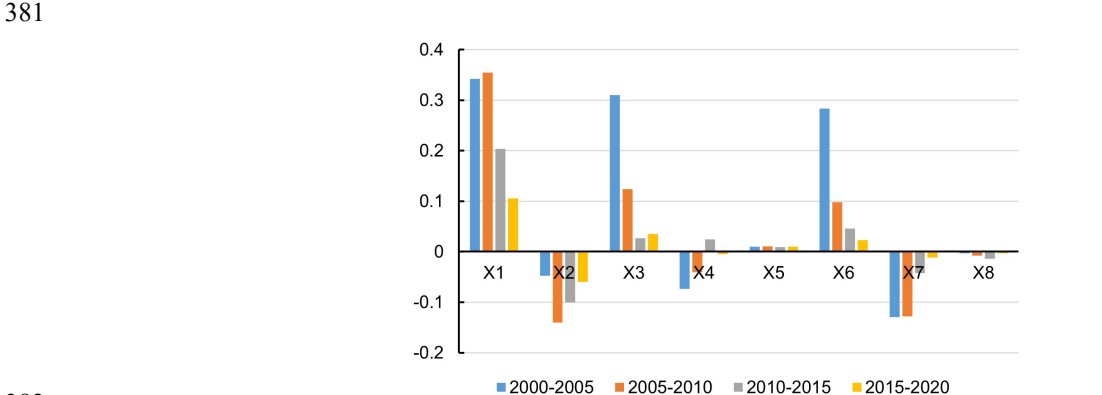
### 373 TCE Driving Factors

374 The GDIM is calculated by standardizing the data of the previous year as a base period in the form of ratios, such  
 375 as 2005 relative to 2000 and 2010 relative to 2005, so this process involves four periods in total from 2000 to 2020,  
 376 where the relative changes are computed and subsequently subtracted by one to derive the rate of change. In Vaninsky's

377 method, Simpson's integration technique is employed for integrating formula (24), a final accuracy up to  $10^{-7}$  (adjusted  
 378 according to device specifications). Furthermore, it is essential that the sum of contributions from calculating various  
 379 factors on TCE changes equals the actual rate of change for verification purposes, as demonstrated in Table 5.

380 **Table 5** Rate of TCE changes and calculation verification

Stage	2000-2005	2005-2010	2010-2015	2015-2020
Sum Rate of Change Test	0.6912748	0.2707408	0.1533793	0.09466727
Actual Rate of Change	0.6912724	0.2707383	0.1533763	0.09466601



382 **Fig. 13** Contributions of various indicators to the rate of TCE change

383 The contribution of each indicator to the  $10^4$  tons of TCE changes can be determined by multiplying the  
 384 corresponding base year TCE with their respective contributions to the rate.

386 **Table 6** Changes in TCE and calculation verification

Stage	2000-2005	2005-2010	2010-2015	2015-2020
Sum of Changes Test	30447.87	20168.49	14519.20	10335.86
Actual change amount	30447.76	20168.30	14518.91	10335.72

387 **Table 7** Contribution of various indicators of TCE at different stages

Stage	2000-2005	2005-2010	2010-2015	2015-2020
X1 Contribution	15068.38	26393.57	19275.91	11540.35
X2 Contribution	-2100.98	-10434.59	-9518.58	-6533.81
X3 Contribution	13655.16	9256.87	2546.29	3872.48
X4 Contribution	-3241.54	-3028.60	2283.82	-534.40
X5 Contribution	439.66	793.42	883.03	1069.69
X6 Contribution	12487.39	7323.97	4365.37	2469.35
X7 Contribution	-5716.98	-9545.76	-3976.14	-1230.51
X8 Contribution	-143.24	-590.39	-1340.51	-317.29

388 The results obtained from GDIM consist of multiple indicator factors, with the essence lying in comparison. If  
 389 only one calculation is conducted, the interpretation of the results necessitates a comparative analysis across multiple  
 390 factors. In case multiple calculations are performed at different periods, comparison remains essential, however, it must  
 391 be based on a consistent standard to ensure meaningfulness.

392 Through GDIM, we could observe that the growth rate of TCE changes is gradually decreasing, resulting in a  
 393 convergence towards zero for various indicators (after subtracting 1). The quantity of TCE exhibits a tendency towards  
 394 relative stability, aligning with the logarithmic function depicted in Fig. 4, Fig 5.

397 The economic development of Shandong Province is still intricately linked to energy consumption, with both  
398 GDP and energy consumption playing significant roles in the TCE. While per capita carbon emissions intensity is  
399 declining, given the province's large population base, most individuals have lower TCE than the average per capita  
400 level. Therefore, a small portion of the population should be primarily responsible for contributing to TCE. Considering  
401 land cover change in Fig. 2, efforts to control carbon reduction should not focus on agricultural land or rural areas that  
402 serve as major food production regions. On the contrary, it is imperative to explore optimization strategies for  
403 individuals and industries characterized by high economic and energy consumption.

404 The primary adverse influencing impacts on TCE encompass economic carbon intensity, energy carbon intensity,  
405 and per capita GDP. Enhancing the overall welfare of residents and expediting the reduction of energy dependency in  
406 economic development are crucial for achieving carbon emissions reduction. However, from 2000 to 2020, population  
407 control measures remained stable with minimal fluctuations in population size, resulting in a diminished contribution.  
408 The consequences following the relaxation of birth control policies still require further investigation in China.

#### 409 Further insights of this study

410 In LISA, it is imperative to acknowledge that the significance threshold at 0.05 should not be rigidly confined to  
411 this exact value. For instance, a marginally larger value such as 0.051, while still in proximity, cannot be entirely  
412 disregarded. Consequently, values equal to or below 0.05 are deemed significant, indicating an actual significance level  
413 lower than 0.05 and a confidence level exceeding 95% (Inequality is more appropriate). This presents a more stringent  
414 argument concerning the treatment of significance or confidence levels in practical scenarios.

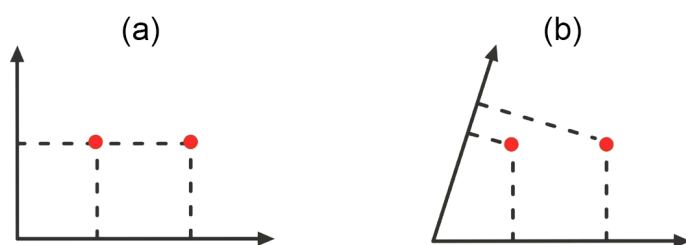
415 In particular, formula (24) in GDIM is a projection operator, and we will discuss the spatial representation here.  
416 Variously, the representation of spatial dimensions should not be limited to the conventional vertical coordinate axis,  
417 similar to a two-dimensional plane, each point can also be depicted using two intersecting axes at angles such as 45°  
418 or other orientations. Moreover, we can even eliminate the use of straight lines as coordinate axes. However, this  
419 alternative approach may pose challenges due to its inconvenience and unfamiliarity.

420 (1) The coordinate axis serves solely as a representation of space, rather than serving as its defining factor.

421 (2) Initially, the space encompasses points, lines, surfaces, and solids. Subsequently, coordinate axes are  
422 introduced as a tool to represent these geometric entities within the spatial framework.

423 (3) Space is an objective entity, and the spatial position of each point remains invariant across different  
424 representations. For instance, in Chinese, it is referred to as '苹果' while in English, it is denoted as 'Apple'. However,  
425 its intrinsic nature remains unaltered regardless of the nomenclature employed. These designations are merely human  
426 constructs devised subsequently, the growth of apple did not after the naming of 'apple'.

427 The significance lies in the fact that, for instance, in Fig. 14, when two points (1,2) and (2,2) are orthogonally  
428 projected onto the y-axis in the case that the  $x$  and  $y$  coordinate axes are orthogonal, their projections will yield identical  
429 values of 2. Consequently, these two points cannot be discerned from each other. However, if we introduce an  
430 inclination to the  $y$ -axis and subsequently project the aforementioned points vertically onto it once more, their  
431 respective  $y$ -coordinates will no longer overlap thereby enabling differentiation between them.



432  
433 **Fig. 14** Comparison of different spatial representations

#### 434 Uncertainty and prospects

435 This study also exhibits certain limitations that could be further enhanced. In terms of data acquisition, the  
436 estimation of carbon emissions currently relies primarily on rough calculations, employing multiplication and  
437 accumulation of carbon emission factors as the primary method. Consequently, the accuracy of estimation heavily

438 hinges upon the precision of upstream data sources. For instance, if land cover accuracy stands at 80% and carbon  
439 emission factor accuracy at 90%, then the estimated accuracy for carbon emissions would approximate to 72%. In  
440 addition, carbon emissions can arise from factors such as the cultivation of different crops and varieties on the same  
441 farmland. It is important to note that the carbon emission factor provides a broad overview of carbon emissions across  
442 various land types, and its application may have some influence on estimation values. While the method based on  
443 carbon emission factors is more suitable for large-scale regions, its applicability in local areas may be relatively limited.

444 **Suggestions and opinions**

445 Taking into account the identified limitations in this study, valuable insights can be gained from these experiences,  
446 which can inform future research endeavors.

447 Firstly, despite potential flaws in the calculation method of carbon emissions, as long as consistent methodology  
448 is employed to determine emissions across different time periods and adheres to standardized criteria with comparable  
449 margins of error, it remains representative for analyzing temporal and spatial variations. Secondly, the primary focus  
450 of this study lies in carbon emissions, the content is comparatively elementary, in the future, it is anticipated that a  
451 more comprehensive correlation analysis will be established, such as detection method SVCP (Xing et al., 2021) for  
452 land cover changes and other relevant factors. Thirdly, due to the utilization of a 5-year timeframe in this study, the  
453 temporal resolution is relatively limited, thereby resulting in a diminished capacity to discern local variations. In  
454 subsequent research endeavors, it would be advantageous to conduct more intricate spatiotemporal pattern mining  
455 based on enhanced temporal resolution.

456 **Conclusions**

457 After conducting carbon emissions calculations, this study employs spatial statistics and factor decomposition  
458 techniques by GDIM. These are a novel approach akin to proof by contradiction or indirect, and presents more rigorous  
459 and innovative arguments for the confidence or significance level, as well as spatial representation in geometry. Based  
460 on this premise, using Shandong Province as a case study, the spatiotemporal distribution pattern and factors  
461 influencing carbon emissions were analyzed to provide valuable insights for carbon reduction strategies.

462 Through analysis, it can be deduced that: (1) In terms of comprehensive strategies for carbon emission reduction,  
463 although the decrease in cropland area directly contributes to DCE reduction, it poses challenges to food security  
464 strategies. Furthermore, given the increase in ICE caused by human activities, emphasis should be placed on addressing  
465 ICE, which also exhibits a logarithmic development pattern for TCE; (2) When formulating regional carbon emission  
466 reduction strategies, priority should be given to inland areas rather than peninsula regions. Particular attention should  
467 be directed towards the primary and secondary echelons at the city level while implementing targeted measures at the  
468 county level based on the current distribution pattern. And it is worth noting that the county scale already encompasses  
469 a significant portion of TCE's true impact range. While TCE exhibits an overall random distribution pattern, it is  
470 important not to overlook the presence of clusters and outliers. Conducting further on-site investigations can provide  
471 detailed insights into the region and facilitate the identification of appropriate measures to address these patterns; (3)  
472 In the case of Shandong Province, GDP and energy consumption are identified as the primary drivers of TCE growth.  
473 The economic expansion in this region is partially reliant on energy consumption, while factors such as economic  
474 carbon intensity, energy carbon intensity, and per capita GDP exert negative influence. To effectively manage TCE  
475 growth, it is imperative to foster the development of a low-carbon economy, enhance social welfare provisions, and  
476 implement appropriate controls targeting high-carbon emitting individuals and industries. It is crucial to shift the focus  
477 of carbon emission reduction efforts away from rural areas and grain-producing regions to ensure food security.

478 In order to achieve the harmonious development between humans and the environment, promote sustainable  
479 development, and mitigate carbon emissions, this long-term global issue necessitates collaborative efforts from all  
480 regions for mutual benefit. This matter is not only pertinent to Shandong Province but also holds significance for  
481 various parts of the world and the future of humanity and our planet.

482 **References**

- 483 Anselin, L. (1995). Local indicators of spatial association—LISA. *Geographical analysis*, 27, 93-115.  
484 <https://doi.org/10.1111/j.1538-4632.1995.tb00338.x>

- 485 Anselin, L. (2010). Thirty years of spatial econometrics. *Papers in Regional Science*, 89, 3-25.  
 486 <https://doi.org/10.1111/j.1435-5957.2010.00279.x>
- 487 Ajmi, A. N., Hammoudeh, S., Nguyen, D. K., & Sato, J. R. (2015). On the relationships between CO<sub>2</sub> emissions,  
 488 energy consumption and income: the importance of time variation. *Energy Economics*, 49, 629-638.  
 489 <https://doi.org/10.1016/j.eneco.2015.02.007>
- 490 Baker, H. S., Millar, R. J., Karoly, D. J., Beyerle, U., Guillo, B. P., Mitchell, D., Shiogama, H., Sparrow, S.,  
 491 Woollings, T., & Allen, M. R. (2018). Higher CO<sub>2</sub> concentrations increase extreme event risk in a 1.5 °C  
 492 world. *Nature Climate Change*, 8, 604-608. <https://doi.org/10.1038/s41558-018-0190-1>
- 493 Chuai, X., Huang, X., Wang, W., Zhao, R., Zhang, M., & Wu, C. (2015). Land use, total carbon emissions change  
 494 and low carbon land management in Coastal Jiangsu, China. *Journal of Cleaner Production*, 103, 77-86.  
 495 <https://doi.org/10.1016/j.jclepro.2014.03.046>
- 496 Chen, J. D., Fan, W., Li, D., Liu, X., & Song, M. L. (2020). Driving factors of global carbon footprint pressure:  
 497 Based on vegetation carbon sequestration. *Applied Energy*, 267, 11.  
 498 <https://doi.org/10.1016/j.apenergy.2020.114914>
- 499 Chen, J., Zhang, J., Li, J., & Li, S. (2024). Spatio-temporal pattern of carbon emissions and its driving factors in the  
 500 Beijing-Tianjin-Hebei region. *Acta Ecologica Sinica*, 44, 2270-2283.  
 501 <https://doi.org/10.20103/j.stxb.202304290904>
- 502 Fan, W. P., Wang, H. K., Liu, Y., & Liu, H. P. (2020). Spatio-temporal variation of the coupling relationship between  
 503 urbanization and air quality: A case study of Shandong Province. *Journal of Cleaner Production*, 272, 11.  
 504 <https://doi.org/10.1016/j.jclepro.2020.122812>
- 505 Getis, A., & Aldstadt, J. (2004). Constructing the spatial weights matrix using a local statistic. *Geographical  
 506 analysis*, 36, 90-104. <https://doi.org/10.1111/j.1538-4632.2004.tb01127.x>
- 507 Getis, A., & Ord, J. K. (1992). The analysis of spatial association by use of distance statistics. *Geographical analysis*,  
 508 24, 189-206. <https://doi.org/10.1111/j.1538-4632.1992.tb00261.x>
- 509 Gao, P., Yue, S. J., & Chen, H. T. (2021). Carbon emission efficiency of China's industry sectors: From the  
 510 perspective of embodied carbon emissions. *Journal of Cleaner Production*, 283, 9.  
 511 <https://doi.org/10.1016/j.jclepro.2020.124655>
- 512 Guo, A., Niu, L., Liu, P., & Li, Y. (2023). Carbon Emission from Land Use in Urban Agglomeration of the Yellow  
 513 River Basin. *Economic Geography*, 43, 172-178+240. <https://doi.org/10.15957/j.cnki.jndl.2023.09.018>
- 514 Kaya, Y. (1990). Impact of carbon dioxide emission control on GNP growth: interpretation of proposed scenarios.  
 515 Paper presented to the IPCC Energy and Industry Subgroup. Response Strategies Working Group, Paris.  
 516 (mimeo)
- 517 Kasman, A., & Duman, Y. S. (2015). CO<sub>2</sub> emissions, economic growth, energy consumption, trade and urbanization  
 518 in new EU member and candidate countries: a panel data analysis. *Economic modelling*, 44, 97-103.  
 519 <https://doi.org/10.1016/j.econmod.2014.10.022>
- 520 Mitchell, A. (2005). *The Esri Guide to GIS Analysis*, Esri Press
- 521 Ma, X. J., Wang, C. X., Dong, B. Y., Gu, G. C., Chen, R. M., Li, Y. F., Zou, H. F., Zhang, W. F., & Li, Q. N. (2019).  
 522 Carbon emissions from energy consumption in China: Its measurement and driving factors. *Science of the  
 523 Total Environment*, 648, 1411-1420. <https://doi.org/10.1016/j.scitotenv.2018.08.183>
- 524 Mishra, A., Humpenöder, F., Churkina, G., Reyer, C. P. O., Beier, F., Bodirsky, B. L., Schellnhuber, H. J., Lotze-  
 525 Campen, H., & Popp, A. (2022). Land use change and carbon emissions of a transformation to timber cities.  
 526 *Nature Communications*, 13, 12. <https://doi.org/10.1038/s41467-022-32244-w>
- 527 Ran, H. Z., Guo, Z. H., Yi, L. W., Xiao, X. Y., Zhang, L., Hu, Z. H., Li, C. Z., & Zhang, Y. X. (2021). Pollution  
 528 characteristics and source identification of soil metal(lloid)s at an abandoned arsenic-containing mine,  
 529 China. *Journal of Hazardous Materials*, 413, 12. <https://doi.org/10.1016/j.jhazmat.2021.125382>
- 530 Rong, T., Zhang, P., Li, G., Wang, Q., Zheng, H., Chang, Y., & Zhang, Y. (2023). Spatial correlation evolution and  
 531 prediction scenario of land use carbon emissions in the Yellow River Basin. *Ecological Indicators*, 154.  
 532 <https://doi.org/10.1016/j.ecolind.2023.110701>
- 533 Shi, K., Yu, B., Zhou, Y., Chen, Y., Yang, C., Chen, Z., & Wu, J. (2019). Spatiotemporal variations of CO<sub>2</sub> emissions  
 534 and their impact factors in China: A comparative analysis between the provincial and prefectural levels.  
 535 *Applied Energy*, 233-234, 170-181. <https://doi.org/10.1016/j.apenergy.2018.10.050>
- 536 Tang, J. W., Ye, S. F., Chen, X. C., Yang, H. L., Sun, X. H., Wang, F. M., Wen, Q., & Chen, S. B. (2018). Coastal blue  
 537 carbon: Concept, study method, and the application to ecological restoration. *Science China-Earth Sciences*,  
 538 61, 637-646. <https://doi.org/10.1007/s11430-017-9181-x>
- 539 Vaninsky, A. (2014). Factorial decomposition of CO<sub>2</sub> emissions: A generalized Divisia index approach. *Energy  
 540 Economics*, 45, 389-400. <https://doi.org/10.1016/j.eneco.2014.07.008>
- 541 Wang, Q., Jiang, X.-T., & Li, R. (2017). Comparative decoupling analysis of energy-related carbon emission from  
 542 electric output of electricity sector in Shandong Province, China. *Energy*, 127, 78-88.  
 543 <https://doi.org/10.1016/j.energy.2017.03.111>
- 544 Wang, S. J., Huang, Y. Y., & Zhou, Y. Q. (2019). Spatial spillover effect and driving forces of carbon emission

- 545 intensity at the city level in China. *Journal of Geographical Sciences*, 29, 231-252.  
546 <https://doi.org/10.1007/s11442-019-1594-1>
- 547 Wang, Y. N., Niu, Y. J., Li, M., Yu, Q. Y., & Chen, W. (2022). Spatial structure and carbon emission of urban  
548 agglomerations: Spatiotemporal characteristics and driving forces. *Sustainable Cities and Society*, 78, 10.  
549 <https://doi.org/10.1016/j.scs.2021.103600>
- 550 Xing, H., Zhu, L., Niu, J., Chen, B., Wang, W., & Hou, D. (2021). A Land Cover Change Detection Method Combing  
551 Spectral Values and Class Probabilities. *IEEE Access*, 9, 83727-83739.  
552 <https://doi.org/10.1109/access.2021.3087206>
- 553 Xing, H., Zhu, L., Chen, B., Niu, J., Li, X., Feng, Y., & Fang, W. (2022a). Spatial and temporal changes analysis of  
554 air quality before and after the COVID-19 in Shandong Province, China. *Earth Sci Inform*, 15, 863-876.  
555 <https://doi.org/10.1007/s12145-021-00739-7>
- 556 Xing, H. Q., Zhu, L. Y., Chen, B. Y., Zhang, L. G., Hou, D. Y., & Fang, W. B. (2022b). A novel change detection  
557 method using remotely sensed image time series value and shape based dynamic time warping. *Geocarto  
558 International*, 37, 9607-9624. <https://doi.org/10.1080/10106049.2021.2022013>
- 559 Yang, J., & Huang, X. (2021). The 30 m annual land cover dataset and its dynamics in China from 1990 to 2019.  
560 *Earth System Science Data*, 13, 3907-3925. <https://doi.org/10.5194/essd-13-3907-2021>
- 561 Yu, S. W., Wei, Y. M., Guo, H. X., & Ding, L. P. (2014). Carbon emission coefficient measurement of the coal-to-  
562 power energy chain in China. *Applied Energy*, 114, 290-300. <https://doi.org/10.1016/j.apenergy.2013.09.062>
- 563 Zhang, Y., & Hong, W. (2024). Spatial-temporal evolution of carbon emissions and spatial-temporal heterogeneity of  
564 influencing factors in the Bohai Rim Region, China. *Environ Sci Pollut Res Int*, 31, 13897-13924.  
565 <https://doi.org/10.1007/s11356-024-32057-y>
- 566 Zhu, L., Xing, H., & Hou, D. (2022). Analysis of carbon emissions from land cover change during 2000 to 2020 in  
567 Shandong Province, China. *Sci Rep*, 12, 8021. <https://doi.org/10.1038/s41598-022-12080-0>
- 568 Zhang, Z., Fu, S., Li, J., Qiu, Y., Shi, Z., & Sun, Y. (2023). Spatiotemporal Analysis and Prediction of Carbon  
569 Emissions from Energy Consumption in China through Nighttime Light Remote Sensing. *Remote Sensing*,  
570 16. <https://doi.org/10.3390/rs16010023>